Case Studies in Chemical and Environmental Engineering 10 (2024) 100877

Contents lists available at ScienceDirect

Case Studies in Chemical and Environmental Engineering

journal homepage: www.sciencedirect.com/journal/case-studies-in-chemical-and-environmental-engineering

Case Report

Jet-fuel range hydrocarbon production from Reutealis trisperma oil over Al-MCM-41 derived from Indonesian Kaolin with different Si/Al ratio

Reva Edra Nugraha [a,b], Didik Prasetyoko [c], Nabila Argya Nareswari [c], Abdul Aziz [c], Holilah Holilah [d], Hasliza Bahruji [e], Muhammad Rahimi Yusop [f], Nurul Asikin-Mijan [f], Suprapto Suprapto [c,*], Yun Hin Taufiq-Yap [g], Aishah Abdul Jalil [h,i], Santi Wulan Purnami [j], Hartati Hartati [k]

[a] Department of Chemical Engineering, Faculty of Engineering, Universitas Pembangunan Nasional "Veteran" Jawa Timur, Surabaya, East Java, 60294, Indonesia
[b] Low Carbon Technologies Research Center, Universitas Pembangunan Nasional "Veteran" Jawa Timur, Surabaya, East Java, 60294, Indonesia
[c] Department of Chemistry, Faculty of Sciences, Institut Teknologi Sepuluh Nopember, Keputih Sukolilo, Surabaya, 60111, Indonesia
[d] Research Center for Biomass and Bioproducts, National Research and Innovation Agency of Indonesia (BRIN), Cibinong, 16911, Indonesia
[e] Centre of Advanced Material and Energy Sciences, Universiti Brunei Darussalam, Jalan Tungku Link, BE 1410, Brunei
[f] Department of Chemical Sciences, Faculty of Science and Technology, Universiti Kebangsaan Malaysia, 43600 UKM Bangi, Selangor, Malaysia
[g] Department of Chemistry, Faculty of Science, Universiti Putra Malaysia, 43400, UPM Serdang, Selangor, Malaysia
[h] Department of Chemical Engineering, Faculty of Chemical and Energy Engineering, Universiti Teknologi Malaysia, 81310, Skudai, Johor Bahru, Johor, Malaysia
[i] Centre of Hydrogen Energy, Institute of Future Energy, Universiti Teknologi Malaysia, 81310, Skudai, Johor Bahru, Johor, Malaysia
[j] Department of Statistics, Faculty of Science and Data Analytics, Institut Teknologi Sepuluh Nopember, Surabaya, East Java, Indonesia
[k] Department of Chemistry, Faculty of Science and Technology, Universitas Airlangga, Surabaya, 60115, Indonesia

ARTICLE INFO

Keywords:
Al-MCM-41
Jet fuel
Catalytic conversion
Si/Al ratio

ABSTRACT

The catalytic conversion of *Reutealis trisperma oil* was carried out over a Al-MCM-41 based catalyst with different Si/Al ratio with no added hydrogen to examine the possibility of the direct production of hydrocarbons in the ranges of jet fuel. In a semi-batch reactor, RTO was combined with 3 % catalyst and heated to 350 °C for 4h. The blank reaction shows the lowest conversion and liquid yield, with values of 39.65 % and 8.74 %, respectively. In contrast, the highest conversion was achieved using the Al-MCM-41 (30) catalyst, and the conversion decreases as the Si/Al ratio of the Al-MCM-41 catalyst increases. Indeed, the mesoporous structure enabled extensive bio-oil diffusion and adsorption, further increasing catalytic conversion. The Al-MCM-41 (30) shows the great performance in catalytic conversion of RTO to hydrocarbon and aromatic chain hydrocarbon. The Al-MCM-41 (30) catalyst resulted in a composition of 41.26 % paraffin, 6.78 % olefin, 21.77 % arenes, and 11.44 % cycloparaffin. This composition is comparable to JP-8 and Jet-A fuels, satisfying the ASTM D7566 standard for aircraft turbine fuel containing synthetic hydrocarbons. The acid site and pore size on the support material influenced the interaction of bio-oil molecules and catalyst which increasing the rate of reactant/product diffusion and improve the jet-fuel production. The obtained results are promising for the use of non-edible RTO and kaolin-derived catalysts in the production of sustainable alternative jet fuels. This approach offers competitive costs and significant environmental and social benefits.

1. Introduction

Jet fuels with tightly regulated qualities are mostly made up of iso-paraffins, n-paraffins, naphthene, olefins, and aromatic components. Additionally, fatty acids and oils can be deoxygenated, hydro-isomerized, and hydrocracked to yield appropriate hydrocarbons within the jet fuel range. The parameters of jet fuel are rigorously defined and include the heating value, viscosity, aromatic content, and the ideal ratio of iso-paraffin to n-paraffin [1]. Jet fuels derived from petroleum have historically provided almost all of the energy needed by the aviation industry, which presents at least two significant issues: (i) Burning fossil fuels releases a significant amount of CO_2, the primary greenhouse gas; (ii) relying only on fuel derived from a finite feedstock has sparked worries about operational costs and future supply security [2]. The

* Corresponding author
E-mail address: suprapto@chem.its.ac.id (S. Suprapto).

https://doi.org/10.1016/j.cscee.2024.100877
Received 12 June 2024; Received in revised form 16 July 2024; Accepted 1 August 2024
Available online 2 August 2024

development of alternative aviation fuels, ideally derived from clean and renewable resources, has become imperative due to these concerns. The choice of feedstock is essential to producing a high-quality biofuel and guaranteeing the process's sustainability. Biomass, encompassing organic materials like plant residues, agricultural waste, and wood chips, is extensively used as the primary feedstock for generating renewable energy such as bioethanol [3,4], biodiesel [5–7], green diesel [8,9], and biochar [10–12], owing to its renewable nature and abundance. Since it eliminates the conflicting interest in the food sector, non-edible plant oil is a preferred feedstock. Tropical countries have an abundance of biomass, thus turning it into biofuel is seen as a path toward sustainable energy [13,14]. Produced in Indonesia, *Reutealis trisperma* oil has been shown to be an appropriate non-edible oil for biofuel conversion [15]. The tree has a long production age [16], can withstand extreme conditions, and can produce seeds that contain up to 52 % triglycerides [17]. High-selective catalysts are needed throughout the Reutealis trisperma oil conversion process to produce liquid hydrocarbon and stop further cracking into uncondensed gases.

Jet fuel is produced from these biomass-based materials using a variety of technologies, including thermochemical and biochemical processes. Alternative fuels for aviation include liquid biohydrogen, biomethane, bioalcohol, hydroprocessed renewable jet fuels (HRJ), and Fischer–Tropsch jet fuels (FTJ) [18]. Hydroprocessed renewable jet fuel has been shown to have the highest jet fuel-to-feed ratio, total energy efficiency, iso-configuration fraction, and saturation degree with a lower percentage of oxygenated chemicals [18,19]. Hydroprocessing technologies, which include hydrotreating, hydrodeoxygenation (HDO), hydrocracking, and isomerization reactions are used to manufacture hydroprocessed renewable jet fuels from oil-based feedstocks. Nevertheless, this process uses a lot of hydrogen to remove double bonds (hydrogenation) and oxygen (hydro-deoxygenation reaction/HDO) from triglyceride oil and to transform to jet-fuel components (hydroisomerization and hydrocracking). In particular, HDO requires more than 300–420 m^3 of hydrogen to remove the oxygen from one m^3 of oil as H_2O [20]. Hydrodeoxygenation uses hydrogen gas at high pressure to reduce oxygenated carbon and unsaturated bonds in biomass, producing a hydrocarbon with a carbon number similar to the precursor of a fatty acid [21].

Accordingly, the non-sulfide catalysts have been reported for catalytic deoxygenation of oil using a limited amount or absence of hydrogen gas. The oxygen in the triglyceride molecule is removed during the catalytic deoxygenation reaction, which also includes decarboxylation and/or decarbonylation (deCOx) reactions. In decarboxylation (DCO_2), oxygen was removed as CO_2 to create a hydrocarbon that had one fewer carbon atom than the fatty acid [22,23]. Deoxygenation can also undergo a decarbonylation (DCO) pathway, in which the oxygen species are removed by releasing carbon monoxide (CO) and water molecules [24]. Since decarboxylation or decarbonylation occurs in the absence of H_2 and at atmospheric pressure, the process is advantageous in reducing the operational cost while operating at safe reaction conditions. DCO_2 and DCO also released a lower amount of water, preventing catalyst deactivation [25]. Nevertheless, the efficiency of deoxygenation processes is hampered by the competing thermal cracking reaction, producing a shorter hydrocarbon chain leading to uncondensed gases and carbonaceous coke.

This study continues our previous work on mesoporous Al-MCM-41 catalysts for vegetable oil conversion into liquid jet-fuel range hydrocarbon via deoxygenation reaction [26,27]. Micro-/mesoporous composite in aluminosilicate structure has been considered a promising material for such catalysts due to the synergistic effect of strong acidity and suitable mesopore structure [28]. The different Si/Al molar ratios have an interesting effect on acidity properties and modify the pore width of the Al-MCM-41 catalyst. The mechanistic reaction pathways over these catalysts are discussed in this paper. The findings may offer a financially viable path for producing jet-fuel hydrocarbon from sustainable non-edible oil resources and offer some guidance on how Al-MCM-41 might be designed in practice for the catalytic hydrodeoxygenation of RTO.

2. Experimental

2.1. Materials

Solid acid catalysts were synthesized using kaolin ($Al_4(Si_4O_{10})(OH)_8$) from Bangka Belitung Island, Indonesia, which included 57 % SiO_2 and 22 % Al_2O_3. TPAOH (40%wt in water) and colloidal silica (LUDOX® HS-40, silica in water at 30 %) were supplied from Sigma Aldrich in Germany. NaOH was acquired from Merck in Germany and CTABr ($C_{19}H_{42}BrN$, assay 99 %) from Applichem. The Reutealis trisperma oil (RTO) as feedstock was acquired from PT. Agrindo Company, Gresik, Indonesia.

2.2. Catalyst synthesis

All solid acid supports were synthesized at Si/Al = 30–90 with the initial molar composition of $10Na_2O{:}xSiO_2{:}\ 2Al_2O_3{:}1800H_2O$ [27]. The gel was created by combining NaOH solution with kaolin and then poured into a bottle made of propylene and stirred for 30 minutes. Following dissolution, 71.9973 g of Ludox and the remaining H_2O distilled water were added to the mixture. Homogenization was then carried out for 8 hours, after which the gel was aged for 6 hours at a temperature of 70 °C. The gel was then subjected to the hydrothermal in an autoclave for 12 hours at 80 °C and 150 °C for 24 h. The solid product was filtered and washed using distilled water until the pH of the supernatant was neutral. The catalyst was dried for 24 hours at 120 °C and calcined at 550 °C (heating rate 2 °C/min) using N_2 atmosphere for 1h and continued with air for 6h. The synthesis was repeated using similar procedure for different Si/Al ratio. The catalysts were denoted as Al-MCM-41 (X) where X is Si/Al ratio of 30, 50, 70, 90.

2.3. Characterization

The phase composition of the solid acid catalyst was analyzed on Bruker type D2 Phaser diffractometer with KFL Cu 2K. The X-ray Diffraction pattern of each sample was measured with a step size of 0.020° and scanning with the range of 2θ = 2–10°. The data were collected with radiation at 10 mA and 30 kV. Binary XPert from Philips using an MPD Cu K diffractometer scanned from 5° to 80° was used to characterize the solid catalysts. The analysis was run at 30 mA, 40 kV with scanned in steps of 0.01670. The functional group was examined utilizing the 400–4000 cm^{-1} spectral range FTIR Shimadzu Instrument Spectrum One 8400S. The Quantachrome Touchwin v1.11 instrument for N_2 adsorption-desorption was used to quantify the surface area and pore volume of the synthesized material. Pyridine-FTIR was used to assess the Lewis and Brønsted acidity (Shimadzu Instrument Spectrum One 8400S). The pyridine desorption was examined at 150 °C for 3h and analyzed using FTIR at 2000-1400 cm^{-1}. The High Transmission-Transmission Electron Microscopy (HT-TEM) of the catalyst was recorded using Hitachi HT-7700 TEM operated at 100 kV. Hitachi Scanning Electron Microscope (SEM) Flex SEM 1000 was used to analyze the morphology of aluminosilicates.

2.4. Catalytic deoxygenation

The RTO deoxygenation was conducted using a semi-batch reactor under N_2 atmosphere. In a 100 mL three-necked flask linked to a distillation apparatus with a stirring heating mantle, oleic acid (10 g) and 3 % catalyst were added. No solvent is used in the deoxygenation reaction. The mixture was stirred continuously throughout the reaction while being heated to 350 °C. The blank reaction in this study was carried out with the same parameter as the catalytic deoxygenation reaction. The deoxygenation reaction was conducted for 4h and was

analyzed with HP 6890 GC (GC-MS/Gas Chromatography-Mass Spectroscopy). Capillary column HP-5MS was utilized; its dimensions were 30 m in length, 0.32 mm in diameter, and 0.25 mm in thickness. For the quantitative study, 1-bromohexane was used as an internal standard. The product selectivity was quantified based on the GC peak area of the desired product over the total peak area according to Eq. (1). Note that the selectivity is an approximation only based on product identification using mass spectroscopy.

$$Selectivity = \frac{Peak\ area\ of\ desired\ compound}{Total\ peak\ area} x100\% \quad \text{(Eq. 1)}$$

The quantity of oxygenated compound in RTO and the liquid product was used to calculate the degree of deoxygenation (DOD), as shown in Eq. (2).

$$Degree\ of\ Deoxygenation\ (DOD) = \left(1 - \frac{\%\ Oxygenated\ compound\ in\ liquid\ product}{\%\ Oxygenated\ compound\ in\ reactant}\right) x\ 100\% \quad \text{(Eq. 2)}$$

The efficiency of the deoxygenation reaction was determined by the percentage of liquid yield obtained after 4h of reaction, relative to the initial weight of RTO oil (Eq. (3)).

$$Liquid\ yield = \frac{Weight\ of\ liquid\ product}{Weight\ of\ RTO\ oil} x\ 100\% \quad \text{(Eq. 3)}$$

3. Results and discussion

3.1. XRD analysis

In this research, wide angle XRD analysis was carried out at an angle of 2θ = 5-50° and a low angle at 2θ = 1.5–10° to identify the sample phase. The X-ray diffraction patterns for all samples are shown in Fig. 1. Wide angle XRD analysis shows that the diffraction peak 2θ = 15°–30° indicates the presence of an amorphous phase in MCM-41 and Al-MCM-41 [26,29]. Low angle XRD analysis in Fig. 1 shows the characteristic diffraction peak at 2θ = 1.5–10° of all samples. This is in line with the characteristics of Al-MCM-41 which has three diffraction peaks at (100), (110), and (200). It can be seen that the peak 2θ = 2.1° indicates a high and strong (100) diffraction plane, there are also two weak peaks at 2θ = 3.6°–4.2° which are related to the reflection of the (110) and (200) planes. These peaks confirm the formation of a highly ordered mesoporous hexagonal structure of Al-MCM-41 [8]. The diffractogram pattern given shows that the increasing Si/Al ratio indicates the more regular and stable the Al-MCM-41 mesoporous structure, this is in accordance with the previous study that as the Si/Al ratio decreases, reflections in the (110) and (200) diffraction planes become less intense and broader, which means that the incorporation of Al into the silica framework still disrupts the long-range order of Al-MCM-41 [30].

3.2. FTIR analysis

FTIR spectra are useful for determining the existence of functional groups in compounds based on the specific chemical bond All catalysts exhibit a wide absorption peak at 3440 cm^{-1} which corresponds to the hydroxyl stretching band for both silanol Si–O–H and adsorbed water molecule on the surface (Fig. 2a) [31]. The absorption peak in the 2932 and 2840 cm^{-1} area is due to asymmetric and symmetric stretching CH_2 vibrations of the alkyl chain from surfactant molecules that have not been calcined [32]. The specific stretching vibration from Si–O–Al framework Al-MCM-41 was displayed in Fig. 2b. The absorption areas around 1224 and 1054 cm^{-1} are attributed to the internal and external stretching of the asymmetric vibrations of the Si–O-T group where T is the Si or Al atom. The peak at a wavenumber of 792 cm^{-1} indicates the bending vibration of the Si–O–Si group. The peak at the wavenumber at 460 cm^{-1} is caused by the bending vibration of T-O where T is a Si or Al atom. This vibration shows the existence of T-O bond vibrations from SiO_4 and AlO_4 tetrahedral groups. Meanwhile, the higher intense absorption peak as an increasing Si/Al ratio was found at 963 cm^{-1} which corresponds to the C–N^+ stretching band from CTAB.

3.3. Textural properties

The nitrogen adsorption-desorption isotherm of Al-MCM-41(X) and MCM-41 commercial catalyst show a type-IV isotherm with H-1-type and H3-type hysteresis loop respectively (Fig. 3a). The H1-type hysteresis loop is typically associated with a combination of cylindrical and parallel plate-shaped pores. Meanwhile, the H3-type hysteresis loop reveals the presence of wedge/slit-shaped pores [33]. These results indicate that Al-MCM-41 has mesoporous material characteristics that match the structure of MCM-41. Type IV isotherm is characterized by the emergence of three adsorption stages, the first is nitrogen being

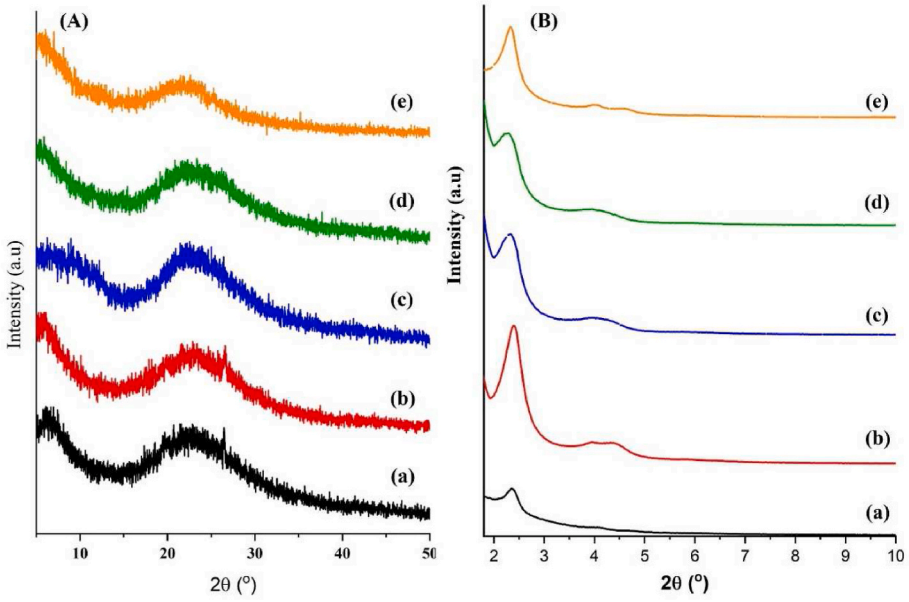

Fig. 1. (A) *Wide angle* and (B) *low angle* diffraction pattern of Al-MCM-41 with S/Al ratio molar of 30 (a), 50 (b), 70 (c), 90 (d) and commercial MCM-41 (e).

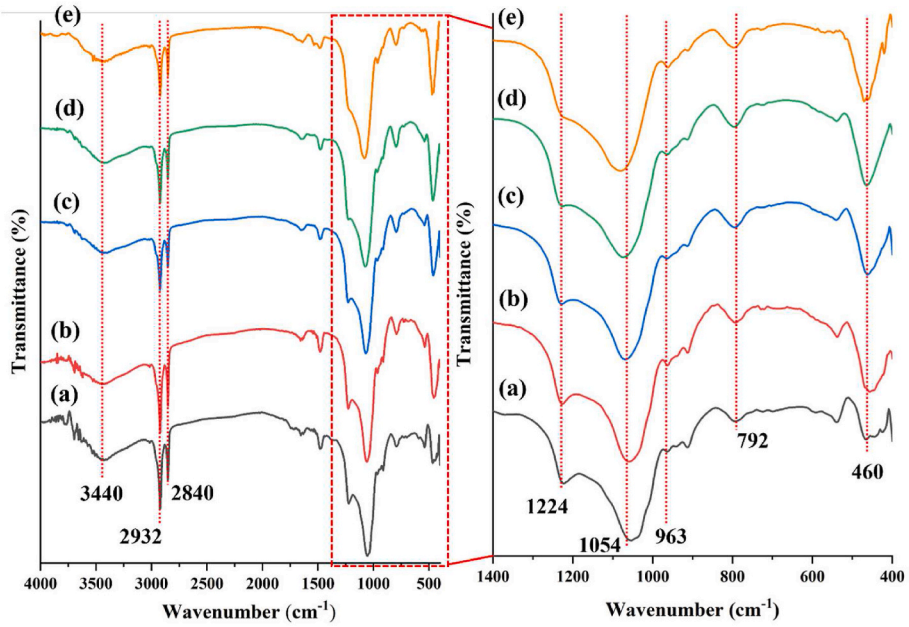

Fig. 2. FTIR spectra of (a) commercial MCM-41, (b) Al-MCM-41 (90), (c) Al-MCM-41 (70), (d) Al-MCM-41 (50), (e) Al-MCM-41 (30).

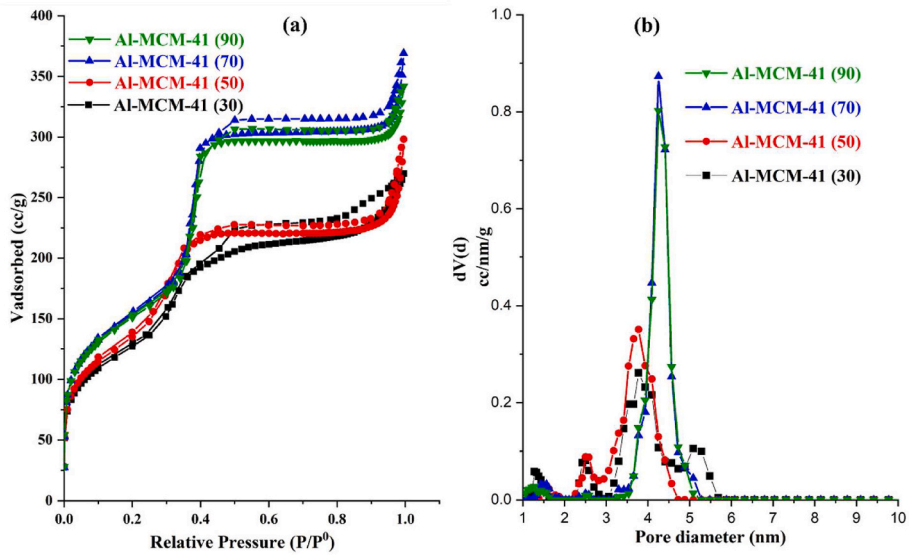

Fig. 3. N_2 adsorption-desorptio[c] isotherm (a) and pore size distributi[c]n (b) of -MCM-41(x) with Si/Al molar r[b]tio of 30, 50, 70 and 9[b].

adsorbed little by little on the surface of the material as the relative pressure P/P0 < 0.3 increases. At this relative pressure, isothermal capillary condensation occurs which begins to fill the multilayer layer. Furthermore, a sharp increase in nitrogen adsorption at a relative pressure of P/P0 = 0.3–0.4 indicates the filling of nitrogen into the mesopores or in other words the formation of a multilayer layer on the pore walls. At relative pressure P/P0 = 0.3–0.4 is also a characteristic type of Al-MCM-41 mesopores. The higher intense N_2 adsorption of

Tabel 1
Textural properties of Al-MCM[b]41(X).

Catalyst	S_{BET}[a] (m^2/g)	S_{micro}[b] (m^2/g)	S_{ext}[b] (m^2/g)	V_{total} (cc/g)	V_{micro}[b] (cc/g)	V^{c}_{BJD}[c] (cc/[a])	D^{b}_{eso}[c] (nm)
Al-MCM-41 (30)	467.17	299.41	146.56	0.388	0.172	0.216	3.775
Al-MCM-41 (50)	522.01	390.57	134.38	0.383	0.191	0.192	3.775
Al-MCM-41 (70)	543.16	359.69	193.96	0.496	0.231	0.265	4.252
Al-MCM-41 (90)	528.92	360.72	181.14	0.472	0.230	0.242	4.252
MCM-41 commercial	377.09	147.73	229.36	0.419	0.063	0.356	2.583

[a] S_{BET} (surface area) by BET method, measured at P/P0 < 0.3.
[b] S_{micro}, S_{ext} and V_{micro} by t-plot method.
[c] V_{meso} and D_{meso} by DFT method.

Al-MCM-41 (70) and Al-MCM-41 (90) at this stage indicate the higher mesopore structure formed. Nitrogen adsorption slightly increases at P/P0 > 0.4 with a hysteresis loop which indicates the presence of mesopores formed inside the particles (intraparticle pore). Structural properties in the form of specific total surface area (S_{BET}), mesopore area (S_{meso}), micropore area (S_{mikro}), mesopore volume (V_{meso}) and pore diameter (D_{meso}) and micropore volume (V_{mikro}) of the Al-MCM-41 sample with varying ratios Si/Al molars 30, 50, 70 and 90 are shown in Table 1. The specific surface area decreases as lowering the Si/Al ratio of Al-MCM-41. The pore size distribution calculated using the DFT method clearly demonstrates the narrow single mesopore diameter for Al-MCM-41 50, 70 and 90 which indicates the average pore diameter could reflect the pore dimension very well (Fig. 3b). Meanwhile, the bimodal pore with lower intensity was formed in the synthesis of MCM-41 commercial and Al-MCM-41 (30).

3.4. Acidity analysis

The surface acidity of the catalysts was determined using FTIR spectroscopy at wave numbers range of 1400–1600 cm^{-1} with pyridine as the probe molecule. Pyridine was utilized as a probe molecule due to the chemical interaction of pyridine with the Lewis and Brønsted acid sites of the catalyst. Nitrogen lone pair in pyridine can interact with the oxide surfaces in three different ways: (i) the nitrogen lone pair of pyridine can be attached to the hydrogen (H-bond) of the weakly acidic surface hydroxyl group resulting in a very weak disturbance in the adsorbed molecule, (ii) if the Brønsted acidity of a surface hydroxyl group is sufficiently high, a proton can be removed, resulting in the creation of pyridinium ions and (iii) nitrogen electrons can interact by donating charge to an unsaturated cation coordinated to the surface referred as Lewis acid [34]. At a wave number around 1447 cm^{-1} is the peak of pyridine interaction with the Lewis acid side of the sample. At this peak, it can be identified that there is an interaction of the nitrogen lone pair in pyridine with the empty orbitals of the metal oxide which results in a shift in the electron density. Meanwhile, the signal at 1550 cm^{-1} is determined to be the peak of pyridine interaction with the Brønsted acid side [35]. On the Brønsted acid side, it appears due to the H^+ ions on the surface of the catalyst being donated to the pyridine molecule to form pyridinium ions ($C_5H_5NH^+$). MCM-41 commercial has Lewis acid sites and very low amount of Brønsted acid sites, while Al-MCM-41 (X) samples have both Lewis and Brønsted acid sites as shown in Fig. 4 and Table 2. It implies that the Al atom enhances the Lewis acid sites on the surface of MCM-41 and provides Brønsted acid sites [36,37]. The total acidity and surface acidity was increased as the decreasing Si/Al in the order of Al-MCM-41 (30) > Al-MCM-41 (50) > Al-MCM-41 (70) > Al-MCM-41 (90) > MCM-41 commercial. The highest amount of Lewis (0.20586 mmol/g) and Brønsted (0.09413 mmol/g) acid sites was determined on Al-MCM-41 (30) since the Al sites in these samples are well-isolated. Nonetheless, the pyridine adsorption capacity was decreased with increasing Si/Al ratio since the Al sites appeared to be poorly separated and aggregated [38].

3.5. Morphology analysis

SEM analysis provided information on the morphology of the MCM-41 commercial and Al-MCM-41 (X). The MCM-41 commercial clearly notes the existence of spherical particles with diameter varies from 0.707 μm to 2.368 μm (Fig. 5a). SEM image of Al-MCM-41 (Fig. 5b–e), functionalization has dramatically altered particle form to non-uniform crystallite structures (0.755–5.621 μm) which slightly larger than pure MCM-41. The EDX analysis of all samples was displayed in Table 3. The Al content was slightly decreased as increasing the Si/Al value which corresponded to the acidity analysis. Fig. 6 shows the TEM analysis of Al-MCM-41 (30) and Al-MCM-41 (70). The transmission electron micrograph of Al-MCM-41 from a cross-sectional view along the [100] axis revealing that the mesoporous material has regular groupings of hexagonal pores in a honeycomb pattern. Meanwhile, in [110] axis revealed the one-dimensionally (1D) channels with a linear array of pores arranged in a hexagonal pattern. The width of the channel from Al-MCM-41 (30) and Al-MCM-41 (70) was calculated using Image-J software which is equal to 3.7 nm and 4.1 nm respectively. These micrographs confirm that the material has a regular pore structure as confirmed by the low angle X-ray diffraction patterns.

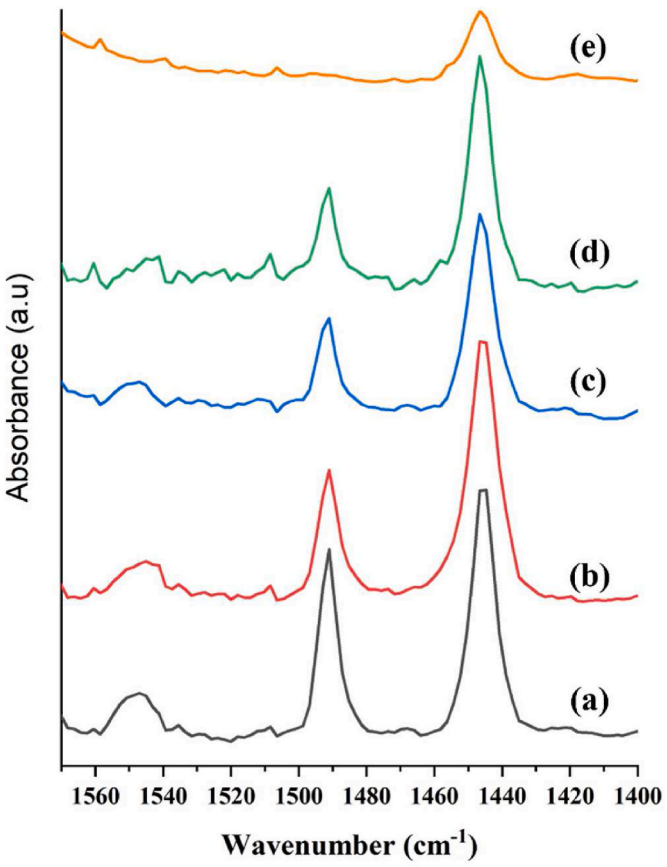

Fig. 4. Pyridine-FTIR spectra of Al-MCM-41 (30) (a), Al-MCM-41 (50) (b), Al-MCM-41 (70) (c), Al-MCM-41 (90) (d) and MCM-41 commercial (e).

Table 2
Acidity analysis of Al-MCM-41 with Si/Al molar ratio of 30, 50, 70, dan 90.

Sample	Acidity (mmol/g)		Total acidity	Surface acidity (mmol/m^2)
	Bronsted	Lewis		
Al-MCM-41 (30)	0.09413	0.20586	0.2999	0.642
Al-MCM-41 (50)	0.03146	0.25974	0.2912	0.558
Al-MCM-41 (70)	0.04507	0.17718	0.2222	0.409
Al-MCM-41 (90)	0.00084	0.2039	0.2047	0.387
MCM-41 commercial	0.00201	0.06574	0.0678	0.180

3.6. Catalytic deoxygenation

Catalytic deoxygenation of *Reutealis trisperma* oil was carried out at 350 °C for 4h using blank reaction, MCM-41 commercial and Al-MCM-41 (X) catalyst. The product of RTO deoxygenation was divided into char and liquid products as shown in Fig. 7a. A blank reaction was conducted with identical reaction conditions to ascertain the distribution of products during RTO deoxygenation without the use of a catalyst. It should be noticed that the blank reaction shows the lowest conversion and liquid yield of 39.65 % and 8.74 % respectively. Meanwhile, the highest conversion was achieved by using the Al-MCM-41 (30) catalyst

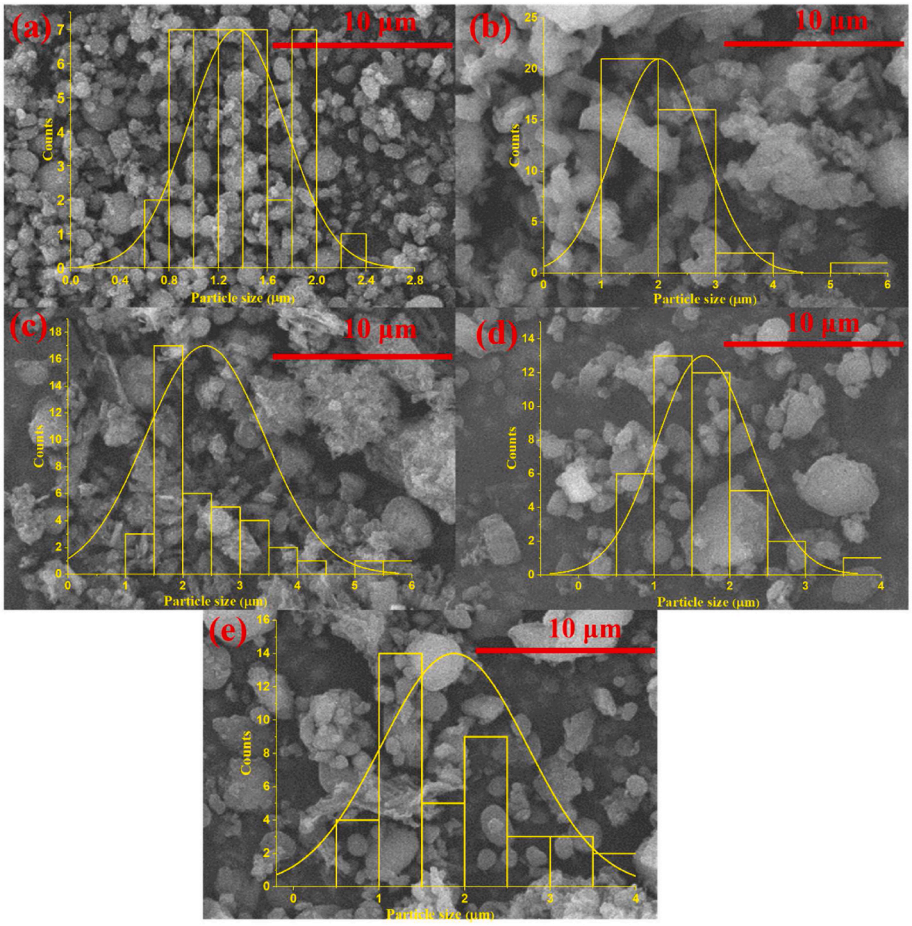

Fig. 5. SEM images of MCM-41 commercial (a), Al-MCM-41 (30) (b), Al-MCM-41 (50) (c), Al-MCM-41 (70) (d) and Al-MCM-41 (90) (e).

Table 3
EDX analysis of Al-MCM-41(X).

Sample	Weight, %		
	O	Al	Si
Al-MCM-41 (30)	50,79	6,93	42,28
Al-MCM-41 (50)	54,96	3,26	41,79
Al-MCM-41 (70)	57,89	3,55	38,57
Al-MCM-41 (90)	53,63	4,23	42,14
MCM-41	55,21	2,75	42,05

and reducing as increasing the Si/Al ratio of the Al-MCM-41 catalyst. This result confirms that the catalyst plays a vital role in enhancing the deoxygenation reaction. Taking into account that the Si/Al molar ratio is a significant parameter for increasing acidity and modifying the pore width of the Al-MCM-41 catalyst [39]. Furthermore, the acid site on the support material influenced the interaction of bio-oil molecules with it. As mentioned in acidity analysis, Al-MCM-41 (30) shows the highest total acidity and surface acidity which contribute to RTO catalytic deoxygenation improvement, which implies the C–C bond dissociation occurred on Lewis sites. However, catalysts with a Si/Al ratio of more than 30 may show a decrease in Al- MCM-41 support's surface area and pore volume. Indeed, the mesoporous structure allowed for deep bio-oil diffusion and adsorption, increasing catalytic conversion even further. In general, the diffusion efficiency between the fluid reactant and the catalyst surface has a significant impact on the generation of liquid products during catalysis. The closer the catalyst pore size is to the molecule of the reactant, the greater the efficiency of liquid mass transfer [40]. Fig. 7b shows the product distribution and degree of deoxygenation of liquid products. The liquid deoxygenated product was classified based on its functional group into hydrocarbon, carboxylic acid, aromatic, cyclic, alcohol and ketone. Theoretically, the deoxygenation reaction removes the carboxyl/carbonyl group fragments from fatty acids to form long and straight-chain hydrocarbons through a decarboxylation/-decarbonylation (deCOx) mechanism [41]. The formation of mono-aromatic compounds involves the dehydrogenation of cycloalkane compounds. Meanwhile, polyaromatics are formed through polymerization and dehydrogenation reactions of mono-aromatic compounds or intramolecular radical cyclization mechanisms [42,43]. The degree of deoxygenation (DOD) was described as the decrement of oxygenated compound concentration in the liquid products relative to the oxygenated concentration in the RTO oil. It can be seen that the blank reaction produces the least amount of hydrocarbon while still containing a substantial amount of carboxylic acid which is most likely derived from the RTO. As a result, it was convincingly established that the deoxygenation reaction is less favorable in the absence of a catalyst [44]. The Al-MCM-41 (30) shows the highest DOD and hydrocarbon yield compared with other catalysts which suggests the major reaction that occurred was decarboxylation/-decarbonylation (deCOx) via C–C scission of triglyceride for oxygen removal [20]. The inclusion of mesopores with widths of 3.70 nm is advantageous for increasing the rate of reactant/product diffusion and improving targeted product production. These reactions were generated by high acidity due to the strong support-metal interaction [28,45]. The higher aromatic compound produced in this catalyst suggests that oligomerizations of aromatics were significantly enhanced over a strong acidic catalyst [46]. Conversely, carboxylic acid becomes the primary product when using MCM-41 commercial catalyst which undergoes thermal cracking into

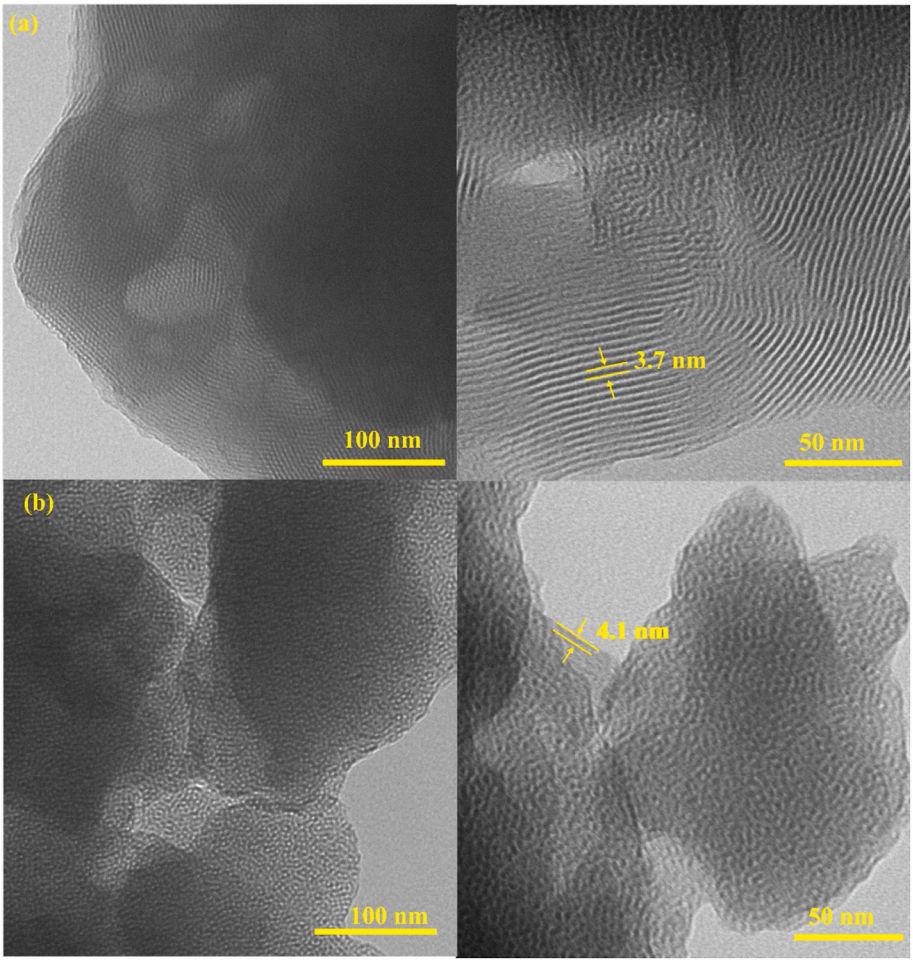

Fig. 6. TEM images of Al-MCM-41 (30) (a) and Al-MCM-41 (70) (b) along the [100] direction (left) and [110] direction (right).

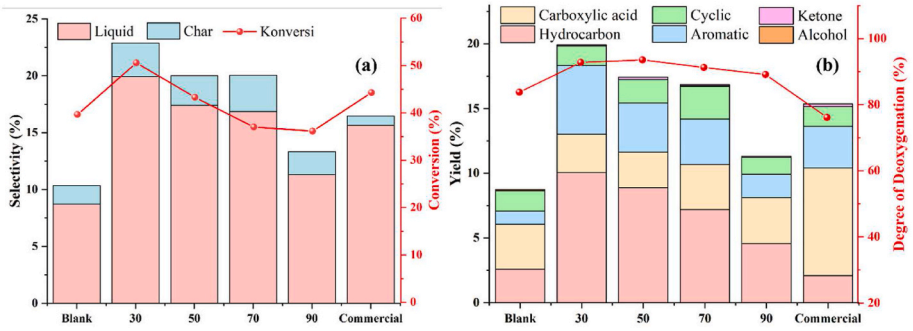

Fig. 7. Conversion and selectivity of product distribution (a) and deoxygenated liquid product distribution of RTO deoxygenation.

short-chain carboxylic acids. Competition between hydrocarbon formation and carboxylic acid can be seen during the reaction. The degree of deoxygenation and hydrocarbon yield decreased dramatically to approximately 76 % and 14 % for MCM-41 commercial.

Fig. 8a shows the hydrocarbon distribution in the liquid products to gasoline ($C_{4\text{-}8}$), jet-fuel ($C_{9\text{-}15}$) and diesel ($C_{16\text{-}18}$) range hydrocarbon. The formation of jet-fuel $C_{9\text{-}15}$ hydrocarbon is significantly increased (77–89 %) and further restricted the formation of diesel range $C_{16\text{-}18}$ hydrocarbon and gasoline range $C_{4\text{-}8}$ hydrocarbon. This implies that the majority reaction that occurred in RTO deoxygnation was the decarboxylation/-decarbonylation (deCOx) reaction to produce straight long-chain hydrocarbon and inhibit the cracking reaction to produce short-chain hydrocarbon. The hydrocarbons are further classified as saturated (C–C) and unsaturated (C=C/C ≡ C) molecules as shown in Fig. 8b. The selectivity of saturated hydrocarbon (paraffin) was higher than unsaturated hydrocarbon (olefin) under all catalysts tested which implies that indirect decarboxylation and direct hydrogenation become the dominant reaction in RTO deoxygenation to produce alkane hydrocarbon [47,48]. Jet fuel's oxidative stability and sealing performance are enhanced by an increase in aromatic concentration [40]. Meanwhile, the selectivity of unsaturated hydrocarbon of 11–20 % was significantly lower than saturated hydrocarbon which suggests the cracking reaction of unsaturated hydrocarbon to generate smaller hydrocarbons or non-condensable gasses may occur. Olefin is known to be more prone to cracking reactions than paraffin, increases the polymerization and prone to degrade during storage. Jet fuel products high in olefins ought to be

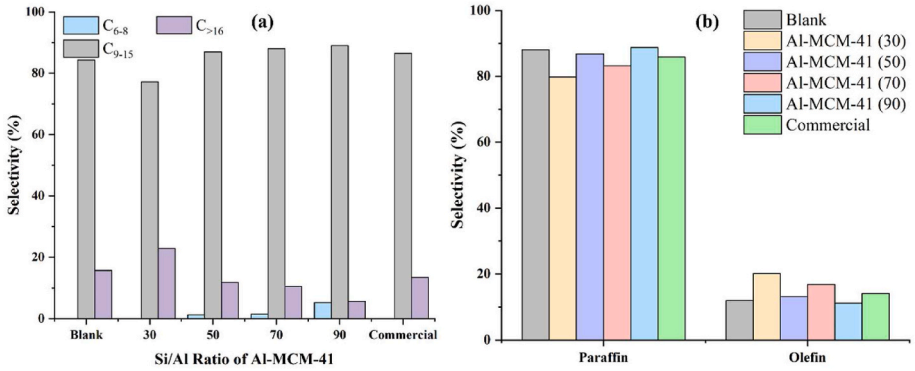

Fig. 8. Hydrocarbon range (a) and alkene/alkane aliphatic hydrocarbon (b) distribution of liquid product.

avoided because they will oxidize fuel [40].

3.7. Production of $C_{9\text{-}15}$ jet-fuel

Jet fuel typically contains a variety of compounds such as 60 % paraffin, 20 % cycloparaffin, and 20 % arenes. The major products observed throughout the reactions were linear alkanes, cycloparaffin, olefins and arenes compounds (Fig. 9). This tendency suggests that olefins, which are involved in secondary reactions leading to the formation of aromatic compounds via dehydrogenation of cyclic compounds produced as intermediates, could be one of the primary products of the thermal and/or catalytic decomposition of triglycerides [49]. Paraffins and cycloparaffins make up the majority of jet fuel (about 70–85 %), and they are primarily in charge of lowering the fuel's freezing point. The ratios of heat to weight and hydrogen to carbon may be lowered by cycloparaffins. It also lowers the gasoline freezing point, a crucial factor for safe fuel use during high-altitude aviation [50]. A lower Si/Al ratio of Al-MCM-41 resulted in greater yields and selectivity of desired compounds for jet fuel formulation. The total selectivity of cycloalkanes, arenes, alkene and alkene slightly reduces followed by an increasing Si/Al ratio of Al-MCM-41 which contributes to the weaker acidity of the catalyst. Alkene formation from cracking reaction and dehydrogenation aromatization to produce arenes occurred at Brønsted acid sites. Meanwhile, cycloalkane formation through Diels-Alder cyclization took place at Lewis acid sites. Thus it can be concluded

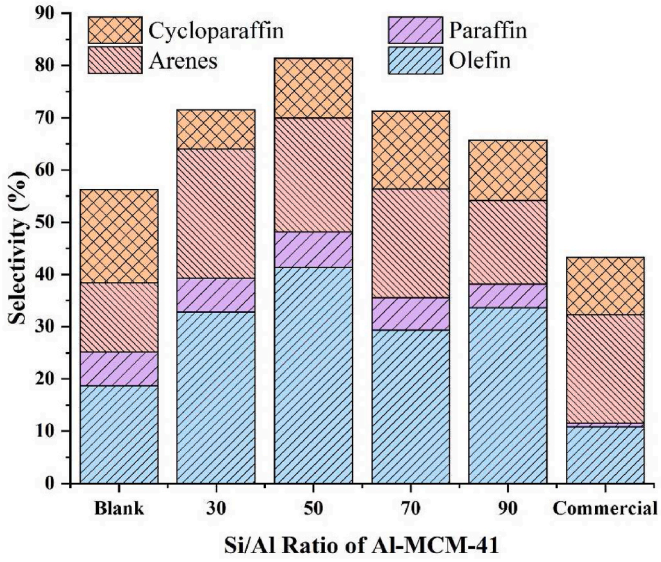

Fig. 9. Selectivity of jet fuel range hydrocarbons converted from RTO Al-MCM-41 (X) and MCM-41 commercial.

that the generation of jet-fuel compounds is influenced by both Brønsted and Lewis acidity [28]. Furthermore, the pore size of 3.7 nm of Al-MCM-41 (30) facilitated the formation of the highest selectivity of the jet-fuel component from RTO deoxygenation over the other catalyst with the pore size of 4.2 nm or 2.5 nm. It has been concluded that for Al-MCM-41 catalysts, not only pore size but also a greater number of acid sites are crucial in increasing reactivity [1].

The fuels derived from biomass, including vegetable oils, are anticipated to have a comparable hydrocarbon distribution to jet fuel derived from petroleum. Table 4 shows the comparison of product distribution of jet fuel range $C_{9\text{–}15}$ hydrocarbons over Al-MCM-41-based catalyst and previous study. The Al-MCM-41 (50) shows the highest efficiency in paraffin formation of 82.25 % jet fuel range $C_{9\text{-}15}$ hydrocarbon. The 41.26 % paraffin, 6.78 % olefin, 21.77 % arenes and 11.44 % cycloparaffin were achieved by using Al-MCM-41 (30) catalyst, which was similar to JP-8 and Jet-A which fulfilled the parameters of the ASTM D7566 standard for aircraft turbine fuel that contained synthetic hydrocarbons. This result was in accordance with a previous study using NiMo/USY@Al-SBA-15 catalyst for WCO hydrodeoxygenation/hydrocracking to produce jet-fuel range hydrocarbon which is classified as JP-8 jet fuel [51]. The solvent-less and free-H_2 deoxygenation in this study was expected to be more efficient and flexible route to produce jet-fuel range compared with hydrocracking or hydrodeoxygenation wh[a]ch requires high security and maintenance due to safety concerns (operates at high pressure and temperature) [52]. The Al-MCM-41-based catalyst without any metal addition/impregnation shows a good result which is comparable to [b]ther metal/support catalysts.

3.8. Reaction pathway of RTO deoxygenation to jet-fuel

Fig. 10 shows the reaction scheme of this work by using RTO as feedstock and Al-MCM-41-based catalyst. The blank reaction was used in this study to investigate the effect of the absence catalyst in RTO deoxygenation. As reported in the previous study, RTO mainly consists of palmitic acid (C16:0), oleic acid (C18:1) and linoleic acid (C18:2) [56]. In the first reaction pathway, one mol triglyceride of RTO undergoes C–C cracking to form three mol of free fatty acid via β-elimination and H-abstraction. In thermal cracking (absence of catalyst), the free fatty acid will form shorter carboxylic acid (C_2–C_{16}) as mentioned in GC-MS analysis in Fig. 7b. Meanwhile, in the presence of catalyst Al-MCM-41, the C–O bond in carboxylic acid will remove as CO and CO_2 via decarbonylation and decarboxylation pathway to produce olefin and paraffin hydrocarbon. Hydrogenation and dehydrogenation may occur in this reaction to produce olefin/paraffin hydrocarbon. The hydrocarbon was further cracked to produce shorter chain hydrocarbon in the jet fuel range hydrocarbon (C_9–C_{15}). It should be noted that the Al-MCM-41-based catalyst promotes the formation of jet-fuel range hydrocarbon than blank reaction. The thermal cracking in a blank reaction will produce shorter chain hydrocarbon that will undergo to

Table 4
Comparison of hydrocarbon class composition in jet fuel-range hydrocarbons with previous study.

Feedstocb	Catalyst	Reaction	C9-15 hydrocarbon (wt%)				Refs.
			Paraffin	Olefin	Arenes	Cycloparaffin	
RTO[a]	Al-MCM-41 (50)	Deoxygenation	41.26	6.78	21.77	11.44	This study
Methyl palmitate	20%HPW-Ni/MCM-41	Hydrocracking and Isomerization	55.4	4.0	13.9	12.6	[53]
Wood biomass	γ-Al2O3	Pyrolysis and cracking	37.21	2.3	53.26	8.86	[54]
WCO[b]	NiMo/USY@Al-SBA-15	Hydrodeoxygenation and hydrocracking	79.4	–	18.7	1.9	[51]
–	JP-8	–	57.2	–	13.5	21.4	[55]
–	Jet-A	–	57	–	20	20	[55]

[a] *Reutealis trisperma* oil.
[b] Waste cooking oil.

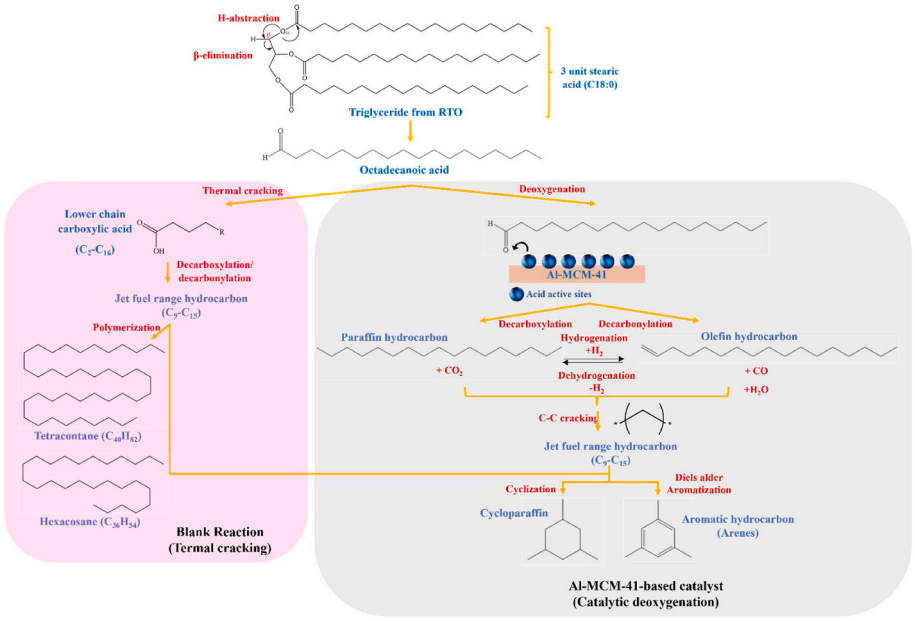

Fig. 10. Proposed reaction mechanism of RTO using blank reaction and Al-MCM-41-based catalyst.

polymerization to produce tetracontane and hexacosane. The cycloparaffin may be produced from cyclization of unsaturated hydrocarbon to form n-cycloalkane [57,58]. The formation of mono-aromatic involves a hydrogenation reaction of cycloparaffin with olefin. Meanwhile, polyaromatic was produced via polymerization and dehydrogenation reaction of monoaromatic or intramolecular radical cyclization [42,43]. Alkenes undergo cyclization and dehydrogenation to produce aromatic hydrocarbons by a Diels-Alder-type mechanism [59].

4. Conclusion

Bio-jet fuel range alkanes were prepared by catalytic deoxygenation reaction of non-edible *Reutealis trisperma* oil without any addition of hydrogen or solvent using a variation of Si/Al ratio of Al-MCM-41 and MCM-41 commercial catalyst. The lowering Si/Al ratio of Al-MCM-41 enhanced the catalytic conversion of RTO and selectivity toward bio-jet fuel components up to 84 %. The pore size and number of acid sites are crucial factors in increasing the reactivity of RTO deoxygenation. The hydrocarbon liquid product is mainly composed of saturated hydrocarbon which suggests that the decarboxylation reaction was the dominant reaction route. Considering that the Si/Al molar ratio is a significant parameter for increasing acidity and modifying the pore width of the Al-MCM-41 catalyst. Additionally, the acid sites on the support material influenced the interaction of bio-oil molecules with the catalyst. This finding indicates that jet fuel can be produced from RTO non-edible oils using Al-MCM-41 in a single-step process, without requiring additional hydrogen or further processing.

CRediT authorship contribution statement

Reva Edra Nugraha: Data curation, Formal analysis, Investigation, Writing- original draft;
Didik Prasetyoko: Conceptualization, Supervision, Validation, Writing - review & editing;
Nabila Argya Nareswari: Data curation, Investigation, Formal analysis, Writing- original draft;
Abdul Aziz: Formal analysis, Writing – original draft;
Holilah Holilah: Validation, Visualization;
Hasliza Bahruji: Validation, Writing - review & editing;
Muhammad Rahimi Yusop: Validation, Writing - review & editing;
Nurul Asikin-Mijan: Supervision, Validation, Writing - review & editing;
Suprapto Suprapto: Supervision, Validation, Funding acquisition, Writing- review & editing;
Yun Hin Taufiq-Yap: Supervision, Writing - review & editing;
Aishah Abdul Jalil: Supervision, Writing - review & editing;
Santi Wulan Purnami: Validation, Writing - review & editing, Supervision;
Hartati Hartati: Validation, Writing - review & editing, Supervision.

Declaration of competing interest

The authors declare that they have no known competing financial

interests or personal relationships that could have appeared to influence the work reported in this paper.

Data availability

Data will be made available on request.

Acknowledgment

The authors acknowledge the Ministry of Education, Culture, Research, and Technology of Republic Indonesia under PDUPT research grant with contract number 1779/PKS/ITS/2024 for funding the research.

References

[1] P. Mäki-Arvela, M. Martínez-Klimov, D.Y. Murzin, Hydroconversion of fatty acids and vegetable oils for production of jet fuels, Fuel 306 (2021), https://doi.org/10.1016/j.fuel.2021.121673.
[2] R.D. Brandão, A.M. de Freitas Júnior, S.C. Oliveira, P.A.Z. Suarez, M.J. Prauchner, The conversion of coconut oil into hydrocarbons within the chain length range of jet fuel, Biomass Convers Biorefinery (2020), https://doi.org/10.1007/s13399-020-01046-9.
[3] J. Chen, B. Zhang, L. Luo, F. Zhang, Y. Yi, Y. Shan, et al., A review on recycling techniques for bioethanol production from lignocellulosic biomass, Renew. Sustain. Energy Rev. 149 (2021) 111370, https://doi.org/10.1016/j.rser.2021.111370.
[4] J. Zhao, Y. Xu, W. Wang, J. Griffin, K. Roozeboom, D. Wang, Bioconversion of industrial hemp biomass for bioethanol production: a review, Fuel 281 (2020), https://doi.org/10.1016/j.fuel.2020.118725.
[5] F. Yaşar, Comparision of fuel properties of biodiesel fuels produced from different oils to determine the most suitable feedstock type, Fuel 264 (2020), https://doi.org/10.1016/j.fuel.2019.116817.
[6] S.Y. Chua, L.A. Periasamy, C.M.H. Goh, Y.H. Tan, N.M. Mubarak, J. Kansedo, et al., Biodiesel synthesis using natural solid catalyst derived from biomass waste — a review, J. Ind. Eng. Chem. 81 (2020) 41–60, https://doi.org/10.1016/j.jiec.2019.09.022.
[7] J. Ching-Velasquez, R. Fernández-Lafuente, R.C. Rodrigues, V. Plata, A. Rosales-Quintero, B. Torrestiana-Sánchez, et al., Production and characterization of biodiesel from oil of fish waste by enzymatic catalysis, Renew. Energy 153 (2020) 1346–1354, https://doi.org/10.1016/j.renene.2020.02.100.
[8] K.B. Baharudin, Y.H. Taufiq-Yap, J. Hunns, M. Isaacs, K. Wilson, D. Derawi, Mesoporous NiO/Al-SBA-15 catalysts for solvent-free deoxygenation of palm fatty acid distillate, Microporous Mesoporous Mater. 276 (2019) 13–22, https://doi.org/10.1016/j.micromeso.2018.09.014.
[9] N.A. Rashidi, E. Mustapha, Y.Y. Theng, N.A.A. Razak, N.A. Bar, K.B. Baharudin, et al., Advanced biofuels from waste cooking oil via solventless and hydrogen-free catalytic deoxygenation over mesostructured Ni-Co/SBA-15, Ni-Fe/SBA-15, and Co-Fe/SBA-15 catalysts, Fuel 313 (2022) 122695, https://doi.org/10.1016/j.fuel.2021.122695.
[10] Q. Zhang, D. Zhang, H. Xu, W. Lu, X. Ren, H. Cai, et al., Biochar filled high-density polyethylene composites with excellent properties: towards maximizing the utilization of agricultural wastes, Ind. Crops Prod. 146 (2020) 112185, https://doi.org/10.1016/j.indcrop.2020.112185.
[11] S. Wijitkosum, Biochar derived from agricultural wastes and wood residues for sustainable agricultural and environmental applications, Int Soil Water Conserv Res 10 (2022) 335–341, https://doi.org/10.1016/j.iswcr.2021.09.006.
[12] B. Mahanty, S. Mondal, Synthesis of magnetic biochar using agricultural waste for the separation of Cr(VI) from aqueous solution, Arabian J. Sci. Eng. 46 (2021) 10803–10818, https://doi.org/10.1007/s13369-021-05572-0.
[13] M.-Y. Choo, L.E. Oi, T.C. Ling, E.-P. Ng, Y.-C. Lin, G. Centi, et al., Deoxygenation of triolein to green diesel in the H2-free condition: effect of transition metal oxide supported on zeolite Y, J. Anal. Appl. Pyrolysis 147 (2020) 104797, https://doi.org/10.1016/j.jaap.2020.104797.
[14] M. Li, S. Xing, L. Yang, J. Fu, P. Lv, Z. Wang, et al., Nickel-loaded ZSM-5 catalysed hydrogenation of oleic acid: the game between acid sites and metal centres, Appl. Catal. Gen. 587 (2019) 117112, https://doi.org/10.1016/j.apcata.2019.117112.
[15] T.M.I. Riayatsyah, H.C. Ong, W.T. Chong, L. Aditya, H. Hermansyah, T.M.I. Mahlia, Life cycle cost and sensitivity analysis of reutealis trisperma as non-edible feedstock for future biodiesel production, Energies 10 (2017) 1–21, https://doi.org/10.3390/en10070877.
[16] K. Kusmiyati, D. Prasetyoko, S. Murwani, M.N. Fadhilah, T.P. Oetami, H. Hadiyanto, et al., Biodiesel production from reutealis trisperma oil using KOH impregnated eggshell as a heterogeneous catalyst, Energies 12 (2019) 2–11, https://doi.org/10.3390/en12193714.
[17] H. Holilah, D. Prasetyoko, T.P. Oetami, E.B. Santosa, Y.M. Zein, H. Bahruji, et al., The potential of Reutealis trisperma seed as a new non-edible source for biodiesel production, Biomass Convers Biorefinery 5 (2014) 347–353, https://doi.org/10.1007/s13399-014-0150-6.
[18] A.A. Ayandiran, P.E. Boahene, A.K. Dalai, Y. Hu, Hydroprocessing of oleic acid for production of jet-fuel range hydrocarbons over cu and fecu catalysts, Catalysts 9 (2019) 13–16, https://doi.org/10.3390/catal9121051.
[19] P. Chintakanan, T. Vitidsant, P. Reubroycharoen, P. Kuchonthara, T. Kida, N. Hinchiranan, Bio-jet fuel range in biofuels derived from hydroconversion of palm olein over Ni/zeolite catalysts and freezing point of biofuels/Jet A-1 blends, Fuel 293 (2021) 120472, https://doi.org/10.1016/j.fuel.2021.120472.
[20] I.H. Choi, J.S. Lee, C.U. Kim, T.W. Kim, K.Y. Lee, K.R. Hwang, Production of bio-jet fuel range alkanes from catalytic deoxygenation of Jatropha fatty acids on a WOx/Pt/TiO2 catalyst, Fuel 215 (2018) 675–685, https://doi.org/10.1016/j.fuel.2017.11.094.
[21] B. Yoosuk, P. Sanggam, S. Wiengket, P. Prasassarakich, Hydrodeoxygenation of oleic acid and palmitic acid to hydrocarbon-like biofuel over unsupported Ni-Mo and Co-Mo sulfide catalysts, Renew. Energy 139 (2019) 1391–1399, https://doi.org/10.1016/j.renene.2019.03.030.
[22] A. Srifa, K. Faungnawakij, V. Itthibenchapong, N. Viriya-empikul, T. Charinpanitkul, S. Assabumrungrat, Production of bio-hydrogenated diesel by catalytic hydrotreating of palm oil over NiMoS2/γ-Al2O3 catalyst, Bioresour. Technol. 158 (2014) 81–90, https://doi.org/10.1016/j.biortech.2014.01.100.
[23] A. Yıldız, J.L. Goldfarb, S. Ceylan, Sustainable hydrocarbon fuels via "one-pot" catalytic deoxygenation of waste cooking oil using inexpensive, unsupported metal oxide catalysts, Fuel 263 (2020) 116750, https://doi.org/10.1016/j.fuel.2019.116750.
[24] S. Janampelli, S. Darbha, Selective deoxygenation of fatty acids to fuel-range hydrocarbons over Pt-MOx/ZrO2 (M = Mo and W) catalysts, Catal. Today 375 (2021) 174–180, https://doi.org/10.1016/j.cattod.2020.04.020.
[25] N. Krobkrong, V. Itthibenchapong, P. Khongpracha, K. Faungnawakij, Deoxygenation of oleic acid under an inert atmosphere using molybdenum oxide-based catalysts, Energy Convers. Manag. 167 (2018) 1–8, https://doi.org/10.1016/j.enconman.2018.04.079.
[26] R.E. Nugraha, D. Prasetyoko, H. Bahruji, S. Suprapto, N. Asikin-Mijan, T.P. Oetami, et al., Lewis acid Ni/Al-MCM-41 catalysts for H2-free deoxygenation of Reutealis trisperma oil to biofuels, RSC Adv. 11 (2021) 21885–21896, https://doi.org/10.1039/d1ra03145g.
[27] R.E. Nugraha, D. Prasetyoko, N. Asikin-Mijan, H. Bahruji, S. Suprapto, Y.H. Taufiq-Yap, et al., The effect of structure directing agents on micro/mesopore structures of aluminosilicates from Indonesian kaolin as deoxygenation catalysts, Microporous Mesoporous Mater. 315 (2021) 110917, https://doi.org/10.1016/j.micromeso.2021.110917.
[28] Z. Zhang, Q. Wang, X. Zhang, Hydroconversion of waste cooking oil into bio-jet fuel over NiMo/SBUY-MCM-41, Catalysts 9 (2019), https://doi.org/10.3390/catal9050466.
[29] N.T.T. Tran, Y. Uemura, S. Chowdhury, A. Ramli, Vapor-phase hydrodeoxygenation of guaiacol on Al-MCM-41 supported Ni and Co catalysts, Appl. Catal. Gen. 512 (2016) 93–100, https://doi.org/10.1016/j.apcata.2015.12.021.
[30] L. Peng, Q. Xie, Y. Nie, X. Liu, M. Lu, J. Ji, Room-temperature production of bio-based aldehydes from vegetable oil-derived epoxide: via H2WO4@Al-MCM-41 as recyclable catalyst, RSC Adv. 9 (2019) 23061–23070, https://doi.org/10.1039/c9ra04348a.
[31] E.P.F. Nhavene, G.F. Andrade, J.A.Q. Arantes Faria, D.A. Gomes, E.M.B. de Sousa, Biodegradable polymers grafted onto multifunctional mesoporous silica nanoparticles for gene delivery, ChemEngineering 2 (2018) 1–16, https://doi.org/10.3390/chemengineering2020024.
[32] R.K. Banjare, M.K. Banjare, S. Panda, Effect of acetonitrile on the colloidal behavior of conventional cationic surfactants: a combined conductivity, surface tension, fluorescence and FTIR study, J. Solut. Chem. 49 (2020) 34–51, https://doi.org/10.1007/s10953-019-00937-4.
[33] W. Uttamaprakrom, P. Reubroycharoen, P. Charoensiritanasin, J. Tatiyapantarak, A. Srifa, W. Koo-Amornpattana, et al., Development of Ni–Ce/Al-MCM-41 catalysts prepared from natural kaolin for CO2 methanation, J. Environ. Chem. Eng. 9 (2021) 106150, https://doi.org/10.1016/j.jece.2021.106150.
[34] A. Penkova, L.F. Bobadilla, F. Romero-Sarria, M.A. Centeno, J.A. Odriozola, Pyridine adsorption on NiSn/MgO-Al 2 O 3 : an FTIR spectroscopic study of surface acidity, Appl. Surf. Sci. 317 (2014) 241–251, https://doi.org/10.1016/j.apsusc.2014.08.093.
[35] F. Gao, Y. Sheng, Y. Song, H. Zou, Sol–gel synthesis of silica composited flower-like microspheres using trivalent europium tartrate as a template, J. Sol. Gel Sci. Technol. 85 (2018) 470–479, https://doi.org/10.1007/s10971-017-4551-4.
[36] J. Li, J. Guo, X. Shi, X. Wen, Y. Chu, S. Yuan, Effect of aluminum on the catalytic performance and reaction mechanism of Mn/MCM-41 for NH3-SCR reaction, Appl. Surf. Sci. 534 (2020) 147592, https://doi.org/10.1016/j.apsusc.2020.147592.
[37] F. Wang, F. Yu, Y. Wei, A. Li, S. Xu, X. Lu, Promoting hydrocarbon production from fatty acid pyrolysis using transition metal or phosphorus modified Al-MCM-41 catalyst, J. Anal. Appl. Pyrolysis 156 (2021), https://doi.org/10.1016/j.jaap.2021.105146.
[38] S.T. Pham, M.B. Nguyen, G.H. Le, T.D. Nguyen, C.D. Pham, T.S. Le, et al., Influence of Brønsted and Lewis acidity of the modified Al-MCM-41 solid acid on cellulose conversion and 5-hydroxylmethylfurfuran selectivity, Chemosphere 265 (2021), https://doi.org/10.1016/j.chemosphere.2020.129062.
[39] H. Taghvaei, A. Moaddeli, A. Khalafi-Nezhad, A. Iulianelli, Catalytic hydrodeoxygenation of lignin pyrolytic-oil over Ni catalysts supported on spherical Al-MCM-41 nanoparticles: effect of Si/Al ratio and Ni loading, Fuel 293 (2021) 120493, https://doi.org/10.1016/j.fuel.2021.120493.
[40] E.S.K. Why, H.C. Ong, H.V. Lee, W.H. Chen, N. Asikin-Mijan, M. Varman, et al., Single-step catalytic deoxygenation of palm feedstocks for the production of

sustainable bio-jet fuel, Energy 239 (2022) 122017, https://doi.org/10.1016/j.energy.2021.122017.
[41] G.A. Alsultan, N. Asikin-Mijan, H.V. Lee, A.S. Albazzaz, Y.H. Taufiq-Yap, Deoxygenation of waste cooking to renewable diesel over walnut shell-derived nanorode activated carbon supported CaO-La2O3 catalyst, Energy Convers. Manag. 151 (2017) 311–323, https://doi.org/10.1016/j.enconman.2017.09.001.
[42] A. Kubátová, J. Šávová, W.S. Seames, Y. Luo, S.M. Sadrameli, M.J. Linnen, et al., Triacylglyceride thermal cracking: pathways to cyclic hydrocarbons, Energy Fuel. 26 (2012) 672–685, https://doi.org/10.1021/ef200953d.
[43] J. Asomaning, P. Mussone, D.C. Bressler, Thermal deoxygenation and pyrolysis of oleic acid, J. Anal. Appl. Pyrolysis 105 (2014) 1–7, https://doi.org/10.1016/j.jaap.2013.09.005.
[44] N.A. Abdul Razak, N.A. Mijan, Y.H. Taufiq-Yap, D. Derawi, Production of green diesel via hydrogen-free and solventless deoxygenation reaction of waste cooking oil, J. Clean. Prod. 366 (2022) 132971, https://doi.org/10.1016/j.jclepro.2022.132971.
[45] Z. Zhang, X. Zhang, Q. Wang, Influence of impurities and oxidation on hydroconversion of waste cooking oil into bio-jet fuel, Chem. Eng. Technol. 43 (2020) 273–281, https://doi.org/10.1002/ceat.201900357.
[46] X. Wu, P. Jiang, F. Jin, J. Liu, Y. Zhang, L. Zhu, et al., Production of jet fuel range biofuels by catalytic transformation of triglycerides based oils, Fuel 188 (2017) 205–211, https://doi.org/10.1016/j.fuel.2016.10.030.
[47] M.Z. Hossain, M.B.I. Chowdhury, A.K. Jhawar, W.Z. Xu, P.A. Charpentier, Continuous low pressure decarboxylation of fatty acids to fuel-range hydrocarbons with in situ hydrogen production, Fuel 212 (2018) 470–478, https://doi.org/10.1016/j.fuel.2017.09.092.
[48] L. Hermida, A.Z. Abdullah, A.R. Mohamed, Deoxygenation of fatty acid to produce diesel-like hydrocarbons: a review of process conditions, reaction kinetics and mechanism, Renew. Sustain. Energy Rev. 42 (2015) 1223–1233, https://doi.org/10.1016/j.rser.2014.10.099.
[49] C.A. Scaldaferri, V.M.D. Pasa, Hydrogen-free process to convert lipids into bio-jet fuel and green diesel over niobium phosphate catalyst in one-step, Chem. Eng. J. 370 (2019) 98–109, https://doi.org/10.1016/j.cej.2019.03.063.
[50] S. Khan, A.N. Kay Lup, K.M. Qureshi, F. Abnisa, W.M.A. Wan Daud, M.F.A. Patah, A review on deoxygenation of triglycerides for jet fuel range hydrocarbons, J. Anal. Appl. Pyrolysis 140 (2019) 1–24, https://doi.org/10.1016/j.jaap.2019.03.005.
[51] Z. Zhang, Q. Wang, H. Chen, X. Zhang, Hydroconversion of waste cooking oil into bio-jet fuel over a hierarchical NiMo/USY@Al-SBA-15 zeolite, Chem. Eng. Technol. 41 (2018) 590–597, https://doi.org/10.1002/ceat.201600601.
[52] M. Zhang, X. Han, H. Wang, Y. Zeng, C.C. Xu, Hydrodeoxygenation of pyrolysis oil in supercritical ethanol with formic acid as an in situ hydrogen source over NiMoW catalysts supported on different materials, Sustain. Times 15 (2023), https://doi.org/10.3390/su15107768.
[53] Z. Zhang, J. Cheng, Y. Zhu, H. Guo, W. Yang, Jet fuel range hydrocarbons production through competitive pathways of hydrocracking and isomerization over HPW-Ni/MCM-41 catalyst, Fuel 269 (2020) 117465, https://doi.org/10.1016/j.fuel.2020.117465.
[54] V.V. Kachalov, V.A. Lavrenov, I.I. Lishchiner, O.V. Malova, A.L. Tarasov, V. M. Zaichenko, Scientific bases of biomass processing into basic component of aviation fuel, J Phys Conf Ser 774 (2016), https://doi.org/10.1088/1742-6596/774/1/012136.
[55] C. Zhang, X. Hui, Y. Lin, C.J. Sung, Recent development in studies of alternative jet fuel combustion: progress, challenges, and opportunities, Renew. Sustain. Energy Rev. 54 (2016) 120–138, https://doi.org/10.1016/j.rser.2015.09.056.
[56] R.E. Nugraha, D. Prasetyoko, Hasliza Bahruji, Suprapto Suprapto, Nurul Asikin-Mijan, Oetami T. Prapti, et al., Lewis acid Ni/Al-MCM-41 catalysts for H 2 -free deoxygenation of Reutealis trisperma oil to biofuels, RSC Adv. 11 (2021) 21885–21896, https://doi.org/10.1039/D1RA03145G.
[57] A. Vasseur, J. Bruffaerts, I. Marek, Remote functionalization through alkene isomerization, Nat. Chem. 8 (2016) 209–219, https://doi.org/10.1038/nchem.2445.
[58] S. Fegade, B. Tande, A. Kubátová, W. Seames, E. Kozliak, Novel two-step process for the production of renewable aromatic hydrocarbons from triacylglycerides, Ind. Eng. Chem. Res. 54 (2015) 9657–9665, https://doi.org/10.1021/acs.iecr.5b01932.
[59] T. Pilusa, M. Shukla, E. Muzenda, Pyrolitic tyre derived fuel: a review, in: Int Conf Chem Min Metall Eng (CMME'2013, 2013, pp. 265–268, https://doi.org/10.13140/2.1.4533.1524.